On the Influence of North Pacific Sea Surface Temperature on the Arctic Winter Climate

M. M. Hurwitz [1, 2], **P. A. Newman** [2] and **C. I. Garfinkel** [3]

1 Goddard Earth Sciences Technology and Research (GESTAR), Morgan State University, Baltimore, MD, USA

2 NASA Goddard Space Flight Center, Greenbelt, MD, USA

3 Johns Hopkins University, Baltimore, MD, USA

Differences between two ensembles of Goddard Earth Observing System Chemistry–Climate Model simulations isolate the impact of North Pacific sea surface temperatures (SSTs) on the Arctic winter climate. One ensemble of extended winter season forecasts is forced by unusually high SSTs in the North Pacific, while in the second ensemble SSTs in the North Pacific are unusually low. High – Low differences are consistent with a weakened Western Pacific atmospheric teleconnection pattern, and in particular, a weakening of the Aleutian low. This relative change in tropospheric circulation inhibits planetary wave propagation into the stratosphere, in turn reducing polar stratospheric temperature in mid– and late winter. The number of winters with sudden stratospheric warmings is approximately tripled in the Low ensemble as compared with the High ensemble. Enhanced North Pacific SSTs, and thus a more stable and persistent Arctic vortex, lead to a relative decrease in lower stratospheric ozone in late winter, affecting the April clear–sky UV index at Northern Hemisphere mid–latitudes.

1 Introduction

The severity of Arctic ozone depletion is highly dependent on the evolution of polar lower stratospheric temperature in late winter and spring [WMO, 2011]. In 2011, unprecedented Arctic ozone depletion resulted from a sustained period of below–average temperatures and an extremely isolated polar air mass [Manney et al., 2011]. The cold 2010–2011 winter resulted in a large volume of polar stratospheric clouds (PSCs), and thereby, high levels of activated chlorine that catalytically destroyed ozone in the Arctic lower stratosphere [Manney et al., 2011]. It is important to understand the causes of these 2011 conditions, in order to assess how Arctic ozone and ultraviolet (UV) radiation levels will likely evolve as the abundance of ozone–depleting substances decline.

Hurwitz et al. [2011a] considered possible dynamical causes of the 2011 ozone depletion event. March was the focus of the authors' study, because conditions in the Arctic stratosphere were particularly anomalous during that month. Several causes were rejected: Direct radiative cooling by greenhouse gases was dismissed because cooling of the Arctic lower stratosphere observed during the satellite era [0.17 ± 0.14 K year^{-1}, in the MERRA reanalysis] was too weak to explain the roughly 10 K cooling in 2011. Both El Niño/Southern Oscillation (ENSO) and the quasi–biennial oscillation (QBO) modulate the strength of the Arctic vortex but could not explain the anomalous stratospheric cooling in 2011. Relative strengthening of the Arctic vortex during La Niña events, as observed in 2011, weakens and begins to reverse by March. Similarly, the authors found that relative strengthening of the mid–winter vortex during the westerly phase of the QBO, relatively to the easterly phase, does not persist through March. Furthermore, the structure and magnitude of dynamical anomalies in the Arctic stratosphere were similar in March 1997 and March 2011, two episodes of low temperatures and large ozone losses, despite different phases of the QBO.

Hurwitz et al. [2011a] showed that winters with exceptionally high North Pacific SSTs, including 2010–2011, were often characterized by weak planetary wave driving in mid–winter and by a cold, persistent Arctic vortices, providing the conditions necessary for severe polar ozone loss. Similarly, Jadin et al. [2010] found positive correlations between mid–winter North Pacific SSTs and the strength of the Arctic vortex, using a 50–year meteorological reanalysis

dataset. North Pacific SSTs may affect planetary wave driving by modifying the large–scale circulation. Weakening of the West Pacific (WP) pattern, characterized by positive upper tropospheric ridges in the western and central North Pacific, tends to inhibit planetary wave driving and strengthen the Arctic vortex in winter [Garfinkel and Hartmann, 2008; Orsolini et al., 2009; Woolings et al., 2010; Garfinkel et al., 2010]. North Pacific ridges are an efficient way to reduce planetary wave driving in the Northern Hemisphere because they destructively interfere with the climatological stationary wave pattern [Garfinkel and Hartmann, 2008; Orsolini et al., 2009; Nishii et al., 2010; Garfinkel et al., 2010]. Specifically, ridges in the North Pacific (i.e., weakening of the WP pattern) have been shown to precede prolonged polar stratospheric cooling of up to 6 K [Nishii et al., 2010] and months with very high PSC volumes [Orsolini et al., 2009].

While observational evidence suggests that North Pacific SSTs can affect polar stratospheric conditions, the Arctic winter climate is highly variable and few anomalous cooling events have occurred during the satellite era. Thus, it is not possible to attribute the dynamical cause(s) of a particular event, such as the unusual meteorology and ozone loss observed in 2011. To pinpoint the role of North Pacific SSTs on the Arctic troposphere and stratosphere in winter, the present study compares two ensembles of chemistry–climate model (CCM) simulations forced by composites of observed SSTs, each providing many samples of the atmospheric response to high or low North Pacific SSTs. Section 2 describes the model and experimental set–up. Section 3 will diagnose ensemble mean differences in Arctic geopotential height, eddy heat flux, temperature, ozone and UV index. Also, Section 3 will assess the frequency of strong eddy heat flux events and major sudden stratospheric warmings (SSWs), characterized by a reversal of the climatological westerly zonal winds at 60°N, 10 hPa, in the two ensembles. Section 4 will provide a discussion and summary.

2 Method

The Arctic winter response to changes in North Pacific SSTs is simulated using the Goddard Earth Observing System Chemistry–Climate Model, Version 2 (GEOS V2 CCM). The GEOS V2 CCM couples the GEOS–5 general circulation model (GCM) with a comprehensive stratospheric chemistry module [Bloom et al., 2005; Pawson et al., 2008]. The model has 2° latitude × 2.5° longitude horizontal resolution and 72 vertical layers, with a model top at 0.01

hPa. Predicted distributions of water vapor, ozone, greenhouse gases (CO_2, CH_4, and N_2O) and CFCs (CFC–11 and CFC–12) feedback to the radiative calculations. An earlier version of the GEOS V2 CCM generally performed well in the SPARC CCMVal [2010] detailed evaluation of stratospheric processes, though in the Arctic winter, lower stratospheric temperatures were warm–biased and thus the model tended to underestimate polar ozone loss [see SPARC CCMVal (2010), figures 4.1 and 6.37]. The present formulation of the GEOS V2 CCM is as described by Hurwitz et al. [2011b]. The model formulation includes an updated GCM, with an improved representation of tropical stationary wave patterns, and a new gravity wave drag scheme that allows the model to produce an internally–generated quasi–biennial oscillation (QBO) with realistic periodicity and magnitude.

This study compares two GEOS V2 CCM ensembles, each composed of 40 simulations of an extended Arctic winter season. Each of the 40 pairs of simulations is initialized independently, using a 1st October restart file from a perpetual ENSO neutral (ENSON) simulation [Hurwitz et al., 2011b], and is run through April 30th. The independent set of initial conditions, together with the model's internal QBO, imply that the simulated winter conditions sample the range of possible QBO phases. Both ensembles are forced by greenhouse gas and ozone–depleting substances representative of the 2005 climate [as in Hurwitz et al., 2011b].

The two ensembles differ only by the SST and sea ice boundary conditions imposed north of 20°N. Annually repeating SST and sea ice climatologies are each constructed from the average of two observed winters when North Pacific (40–50°N, 160–200°E) SSTs were either unusually high (1990–1991 and 1996–1997; Figure 1a, blue stars) or unusually low (1986–1987 and 1987–1988; Figure 1a, cyan stars). Note that this experimental design tests the atmospheric sensitivity to changing North Pacific SSTs, rather than the linearity of atmospheric response. South of 20°N, ENSO neutral SST and sea ice climatologies are prescribed in both ensembles [as in the ENSON simulation as described by Hurwitz et al., 2011b]. Using ENSO neutral conditions removes the potential impacts of El Niño and La Niña conditions on the simulated Arctic stratospheric response to unusually high or low North Pacific SSTs. SST and sea ice values are obtained from the HadISST1 dataset [Rayner et al., 2003].

Figure 1b shows the evolution of North Pacific SST differences throughout the extended winter season. High – Low differences increase from approximately 1 K in October to 2 K in January, and gradually decrease to 1 K by the end of each simulation. Note that the seasonal evolution of High – Low SST differences resembles that of the North Pacific SST anomalies during the 2010–2011 winter, though the magnitude of the imposed High – Low SST differences is approximately twice as large. Figures 1c and 1d, respectively, show January/February climatological mean SSTs and High – Low SST differences, in the Pacific sector. In the North Pacific, SSTs range from 5–8°C in the High ensemble (Figure 1c). Positive High – Low differences span the Pacific at mid–latitudes, with negative SST differences along the west coast of North America and Alaska, and in the subtropical western Pacific. Note that the pattern of High – Low SST differences resembles the pattern of SST anomalies observed during the 2010–2011 winter (not shown).

In order to interpret the High – Low differences, simulated stratospheric ozone and temperature fields are compared with observational datasets. Simulated total ozone is compared with the TOMS/SBUV dataset [updated from Stolarski and Frith, 2006]. Simulated temperature fields are compared with the Modern Era Retrospective–Analysis for Research and Applications (MERRA) reanalysis. The MERRA reanalysis is based on an extensive set of satellite observations and on the Goddard Earth Observing System Data Analysis System, Version 5 (GEOS–5) [Bosilovich, 2008; Rienecker et al., 2011]. The MERRA reanalysis has vertical coverage up to 0.1 hPa, and for this study, is interpolated to 1.25° x 1.25° horizontal resolution. Both the TOMS/SBUV and MERRA datasets span the 1979–2011 period.

3 Differences Between the High and Low Ensembles

3.1 Troposphere

Figure 2 shows the evolution of High – Low monthly mean geopotential differences at Arctic latitudes in December and March. At 850 hPa, a region of positive geopotential height differences in the North Pacific, co–located with the region of increased SSTs (see Figure 1d), develops in December (Figure 2a) and persists through the spring (Figure 2d). Positive geopotential height differences are also co–located with the climatological trough in the North Pacific (gray, dashed contours), suggesting that a relative increase in North Pacific SSTs tends to

149 decrease tropospheric wave driving. A region of negative differences develops over the Arctic
150 cap in December (Figure 2a), and persists through the spring (Figure 2d). In January through
151 March, sea level pressure decreases at polar latitudes, and increases in the European and Atlantic
152 sectors, suggest a strengthening of the North Atlantic Oscillation (NAO). Specifically, the sea
153 level pressure difference between 335°E, 37°N (i.e., the Azores High) and 339°E, 64°N (i.e., the
154 Icelandic Low) is significantly different in the High and Low simulations at 95% confidence
155 level in January.
156
157 The tropospheric response to the North Pacific SST difference is structurally barotropic.
158 Consistent with Frankignoul and Sennéchael [2007], upper tropospheric (300 hPa; Figures 2b
159 and 2e) geopotential height differences mimic the near–surface (850 hPa; Figures 2a and 2d)
160 geopotential height differences. From January through March, High – Low differences indicate
161 a strengthening of the Arctic Oscillation: negative differences at Arctic latitudes, and positive
162 differences at mid–latitudes, particularly in the Pacific and Atlantic sectors.
163
164 Eddy heat flux at 40–80°N, 100 hPa is a measure of the planetary wave energy entering the
165 Arctic stratosphere. Time–integrated eddy heat flux in this region is highly correlated with polar
166 lower stratospheric temperatures, with a 1–2 month lag [Newman et al., 2001]. Figure 3 shows
167 the mean eddy heat flux in the preceding 45 days, in the High (blue, upper panel) and Low
168 (cyan) ensembles, as well as the mean differences between the two ensembles (dotted black line,
169 lower panel). High – Low differences are negative and statistically significant from early
170 January through mid–February, suggesting an increase in eddy heat flux in December and
171 January. By early February, eddy heat flux in the Low ensemble is both larger and more variable
172 than in the High ensemble. The sign of High – Low eddy heat flux differences flips in mid–
173 April (lower panel).
174
175 Not only do the 45–day mean eddy heat fluxes differ between the two ensembles, so does the
176 frequency of strong wave events. Table 1 lists the total of days where the eddy heat flux at 40–
177 80°N, 100 hPa is greater or equal to 25 K m s^{-1}. Strong eddy heat flux "events" are defined as
178 the persistence of 40–80°N, 100 hPa eddy heat flux, greater or equal to 25 K m s^{-1}, for two or
179 more consecutive days. The total number of strong eddy heat flux events is larger in the Low

ensemble than the High ensemble, as is the number of strong eddy heat flux days. In December and February, note that the number of strong heat flux days is roughly doubled in the Low ensemble as compared with the High ensemble.

3.2 Polar Stratosphere

Polar geopotential height at 50 hPa is a measure of the strength of the Arctic vortex. Negative High – Low geopotential height differences over the polar cap (Figures 2c and 2f) persist from January through March. Negative geopotential height differences shift toward the Siberian sector in April. Polar cap temperature at 50 hPa is used to examine the seasonal evolution of the High – Low changes. The polar cap cools in the mid– to late winter, in the High ensemble relative to the Low ensemble (Figure 3, lower panel). 50 hPa polar cap temperature differences are statistically significant in January and February, consistent with the negative eddy heat flux differences, and in late March (black and gray Xs below the center panel). Polar cap temperature differences reverse sign in mid–April. Early winter temperature differences are negligible.

Arctic variability is also affected by North Pacific SSTs. In Figure 3 (center panel), blue (cyan) dashed lines indicate the 90^{th}–percentile (fourth–highest) and 10^{th}–percentile (fourth–lowest) temperature values of the High (Low) ensemble. The 10^{th}–percentile values are similar in the two ensembles. However, the 90^{th}–percentile values are significantly warmer (denoted by the Xs above the plot) in the Low ensemble than in the High ensemble in January and early February. This suggests that mid–winter polar stratospheric variability is enhanced when North Pacific SSTs are relatively lower. Section 3.3 will relate this result to the relative frequency of sudden stratospheric warmings (SSWs) in the two ensembles.

The mean and distribution of seasonal mean January–February–March (JFM) polar cap temperature at 50 hPa differs robustly between the two ensembles. Figure 4a shows histograms of the JFM mean polar cap temperature; the mean High – Low difference is 1.91 K. Note the upper tail of temperature values in the Low ensemble (cyan bars). While polar stratospheric conditions depend on the phase of the simulated QBO in early winter (i.e., the Holton–Tan effect), the JFM polar cap temperature at 50 hPa is independent of QBO phase. Figure 4b shows histograms of the JFM temperature partitioned by the magnitude of JFM zonal winds at 30 hPa,

211 between 10°S and 10°N [following Hurwitz et al., 2011b]. QBO–easterly years are
212 characterized by JFM zonal winds greater than 2 m s^{-1}, while QBO–westerly years are
213 characterized by zonal winds less than –2 m s^{-1}; the QBO–E and QBO–W means and
214 distributions are statistically indistinguishable.
215
216 Polar stratospheric temperature anomalies propagate from the upper stratosphere in mid–winter
217 to the lower stratosphere in spring. The evolution of High – Low temperatures at 80°N through
218 the extended winter season is summarized by Figure 5. Temperature differences are negligible
219 in November through mid–December. By late December, relative cooling develops at and above
220 10 hPa. In January, relative cooling of the middle stratosphere exceeds 8 K. The anomalous
221 cooling slowly descends, with weaker cooling extending to the 400–hPa level in February.
222 Lower stratospheric cooling is strongest in March and early April. In March, relative cooling of
223 1–2 K extends to the surface layer, suggestive of downward stratosphere–troposphere coupling.
224 Stratospheric cooling is followed by relative warming of 2–4 K, with an approximately two–
225 month lag.
226
227 Interannual variability of mid–winter North Pacific SSTs explains some of the observed
228 interannual variability in polar lower stratospheric conditions in late winter. Figure 6 shows the
229 observed January/February North Pacific SST index [as in Hurwitz et al., 2011a] as a function of
230 February/March V_{PSC} timeseries for the 380–550 K potential temperature layer, updated from
231 Rex et al. [2004, 2006]. V_{PSC} represents the volume of polar air that is below the formation
232 threshold for polar stratospheric clouds (approximately 195 K at 50 hPa). February/March V_{PSC}
233 is thus a measure of the potential for late winter ozone depletion. The V_{PSC} correlation with the
234 January/February North Pacific SST index is greater for February/March ($r = 0.38$) than for the
235 December–March average ($r = 0.33$; not shown). Furthermore, the SST–V_{PSC} correlations
236 increase when only the largest V_{PSC} values are considered: $r = 0.76$ for February/March $V_{PSC} \geq$
237 15×10^6 km^3; this result is consistent with the finding that blocking in the North Pacific tends to
238 precede very high monthly mean V_{PSC} values [Orsolini et al, 2009]. However, while V_{PSC} and
239 North Pacific SSTs were both unusually high in 2011, North Pacific SSTs do not explain high
240 V_{PSC} values in e.g., 1984 and 2000. In the model simulations, approximately ⅔ of the 40 pairs of
241 simulated winters show a strong High – Low cooling of the polar stratosphere in March.

242

243 **3.3 Sudden Stratospheric Warmings**

244 Major sudden stratospheric warmings (SSWs) are characterized by reversals in the zonal wind
245 direction at 60°N, 10 hPa. The observed occurrence of SSW events, during years when
246 January/February North Pacific SSTs were unusually high or low, is compiled from a list of
247 historical SSWs [Butler and Polvani, 2011]. Distinct zonal wind reversals are required to take
248 place at least 20 days apart and only when distinct from the final warming [Charlton and Polvani,
249 2007]. SSWs occurred during all of the four winters with the lowest North Pacific SSTs between
250 1979 and 2011 (see Figure 1a), while no SSWs were observed during the four winters with the
251 highest North Pacific SSTs. Therefore, the High and Low GEOS V2 CCM ensembles serve to
252 test if this strong observed sensitivity of the SSW frequency to North Pacific SSTs is robust to a
253 larger sample size.

254

255 Table 2 shows the number and frequency of SSWs in the two GEOS V2 CCM ensembles.
256 Simulated SSW identification follows Charlton and Polvani [2007] and Butler and Polvani
257 [2011]. The relative frequency of simulated SSWs is consistent with the mean strength of the
258 Arctic vortex: the frequency of winters with at least one SSW is approximately tripled in the
259 Low ensemble (20 active winters) as compared with the High ensemble (7 active winters). There
260 are two winters each with two SSWs in both ensembles. The increased SSW frequency in the
261 Low ensemble is consistent with the overall increase in variability in January (see Figure 3). The
262 frequency of active winters during perpetual ENSO neutral conditions (10 active winters in a 40–
263 year sample) lies between that for the North Pacific SST extremes.

264

265 The dynamical situation preceding SSWs in the High ensemble is distinct from that preceding
266 SSWs in the Low ensemble. For example, Figure 7 shows composites of the zonally asymmetric
267 component of 300–hPa geopotential height anomalies in the 5–20 days preceding SSWs, at
268 Arctic latitudes. While a blocking high is located in the North Pacific in both ensembles, the
269 High ensemble (Figure 7a) has a wavenumber–2–like structure while the High ensemble has a
270 wavenumber–1–like structure. These structures are, respectively, consistent with the
271 tropospheric precursors preceding split and displacement type SSWs [Charlton and Polvani,
272 2007; Cohen and Jones, 2012].

3.4 High–Latitude Stratospheric Ozone and UV

High – Low ozone differences at 80°N reflect temperature differences at 80°N. Figure 8 shows the slow descent of negative stratospheric ozone differences in January through April, with corresponding positive ozone differences above, and a further layer of negative ozone differences in the uppermost stratosphere. Negative ozone differences are largest at 10 hPa (~0.3 ppmv) and are approximately 0.1 ppmv in the lower stratosphere. The reversal in the sign of High – Low 50–hPa temperature differences in mid–April (see Figures 3 and 5) does not occur in the ozone difference field. Weak, negative ozone differences are seen in the Arctic troposphere in mid–February through March, indicating a downward coupling between the stratosphere and troposphere, as in the 80°N temperature differences (Figure 5).

While High – Low polar ozone differences are consistent with polar temperature differences, ozone differences are small and are generally not statistically significant. Weak polar ozone differences result from a polar lower stratospheric warm bias in the GEOS V2 CCM. Figure 9 shows that the High and Low ensemble mean temperatures at 80°N, 50 hPa remain above the threshold for PSC formation (approximated by the black dotted line), and thus for chemical ozone depletion, throughout the winter. In contrast, observed temperatures during the e.g., 2010–2011 winter (solid black line) dropped below the PSC formation threshold for sustained periods in February and March. However, the area where polar temperatures are below 195 K at 50 hPa (i.e., the approximate area of PSCs, or the potential for ozone depletion), is significantly different in the High and Low ensembles in January, February and March (see Table 3).

In April, High – Low ensemble mean total ozone differences are consistent with the observed total ozone anomalies in 2011. In the GEOS CCM simulations (Figure 10a), positive differences of 5–10 DU are seen in the Canadian sector, while negative differences of up to 37 DU are seen in the European and Siberian sectors. Weaker, negative total ozone differences span the mid–latitude Pacific and the eastern USA. The observed total ozone anomalies in April 2011 (Figure 10b) match the pattern of the simulated differences, but with two main differences: First, the observed anomalies are approximately three times larger. Second, the observed response lacks the simulated negative total ozone response in the mid–latitude East Asia and Pacific sector.

304

305 Decreased total ozone in spring enhances the flux of clear–sky UV radiation to the earth's
306 surface, while increased total ozone diminishes the UV flux. Simulated April UV differences are
307 calculated for four cities: Washington, Calgary, London and Moscow. These cities span the
308 longitudinal circle at northern mid–latitudes. Figure 11 shows the April UV index in the four
309 cities, in two years when North Pacific SSTs were unusually low, three years when North Pacific
310 SSTs were unusually high, as well as the High and Low ensemble mean values. In Washington,
311 London and Moscow, North Pacific SSTs and the April UV index are correlated: UV index is
312 highest when North Pacific SSTs are elevated and Arctic ozone depletion is relatively more
313 severe. The statistical significance of High – Low UV differences is highest for Washington. In
314 Calgary, the UV index exhibits the opposite sensitivity to North Pacific SSTs, consistent with the
315 total ozone response in April.

316

317 **4 Conclusions**

318 GEOS V2 CCM simulations show that SSTs in the North Pacific region significantly affect the
319 Arctic troposphere and stratosphere in winter. Two ensembles, each of 40 extended winter
320 season simulations, differ only by the SST boundary conditions imposed north of 20°N. The
321 largest, positive SST differences are in the North Pacific region. By imposing no tropical SST
322 differences, the impact of ENSO on Arctic winter variability is removed. While the phase of the
323 QBO varies between each of the ensemble members, differences in the simulated Arctic late
324 winter response during QBO–easterly versus QBO–westerly conditions are negligible.

325

326 In the troposphere, enhanced North Pacific SSTs tend to weaken the Aleutian low, inhibiting
327 planetary wave propagation into the stratosphere. An Arctic relative low–pressure center is
328 established from December through March, throughout the tropospheric column. Furthermore,
329 enhanced North Pacific SSTs can affect winter weather in the Northern Hemisphere: relatively
330 lower surface pressure at polar latitudes coupled with relatively higher pressure at mid–latitudes
331 imply a strengthening of the North Atlantic Oscillation and Arctic Oscillation. However, SST
332 differences between the High and Low ensembles are non–zero in the North Atlantic, and thus,
333 imposed Atlantic SST differences may have contributed to the simulated tropospheric response.

334

335 Reduced tropospheric planetary wave driving, in winters with relatively warmer North Pacific
336 SSTs, acts to strengthen the Arctic vortex. Relative cooling of the Arctic stratosphere begins in
337 the upper stratosphere in January and slowly descends to the lower stratosphere by March and
338 early April. The JFM seasonal mean difference in polar cap temperature at 50 hPa is 1.91 K.
339 When North Pacific SSTs are relatively low, not only is the seasonal mean Arctic vortex
340 weakened, the frequency of simulated sudden stratospheric warmings is considerably larger
341 (consistent with Jadin et al. [2010]). Furthermore, the sudden warmings that do occur when
342 North Pacific SSTs are anomalously cool (warm) tend to be associated with wavenumber–1
343 (wavenumber–2).
344
345 The Arctic ozone response to enhanced North Pacific SSTs is consistent with the dynamical
346 response. Relative cooling of the Arctic stratosphere corresponds with a relative decrease in
347 polar ozone. Negative ozone differences begin in late December, around 10 hPa, and descend to
348 the lowermost stratosphere through mid–April. Negative ozone differences are centered over the
349 polar cap from January through March. Positive ozone differences are seen above the region of
350 negative differences. Though the pattern of simulated ozone differences is consistent with the
351 dynamical response, the ozone differences are not statistically significant, likely because of the
352 GEOS V2 CCM's mid–winter warm bias.
353
354 In April, negative High – Low ozone differences shift away from the pole and toward the
355 Siberian sector. The pattern of simulated total ozone differences is similar to the pattern of
356 ozone anomalies observed in April 2011; however, the magnitude of the simulated differences is
357 approximately a third of that observed. In April, negative total ozone differences exceeding 30
358 DU are simulated in Europe and the Siberian sector (leading to small increases in clear–sky UV
359 index in e.g., London and Moscow), while total ozone increases exceed 20 DU over northern
360 Canada (slightly decreasing the UV index in e.g., Calgary). Weaker negative differences are
361 seen at northern mid–latitudes (increasing the April UV index in e.g., Washington).
362
363 The results of the present study suggest that one of the keys to predicting the behavior of the
364 Arctic stratosphere in a future climate is to understand variability and trends in the North Pacific
365 region. Interannual variability in North Pacific SSTs is primarily driven by a "subarctic mode"

366 of decadal variability that is independent of ENSO and the Pacific Decadal Oscillation (PDO)
367 [Nakamura et al., 1997; Frankignoul and Sennéchael, 2007]. However, the IPCC Fourth
368 Assessment report attributes recent warming of the North Pacific upper ocean to the positive
369 phase of the PDO. CMIP5 simulations of likely 21st century climate scenarios will provide
370 updated forecasts of future changes in North Pacific SSTs.
371
372 The above model results support the hypothesis that anomalously warm North Pacific SSTs
373 contributed to the strong and prolonged cooling of the polar lower stratosphere, and severe ozone
374 depletion, that were observed during the 1996–1997 and 2010–2011 winters [Pawson and
375 Naujokat, 1999; Manney et al., 2011; Hurwitz et al., 2011a]. However, elevated North Pacific
376 SSTs alone do not predict polar stratospheric cooling in late winter. January/February North
377 Pacific SSTs are well correlated with late winter V_{PSC}, though some of the "coldest winters"
378 (e.g., 2004–2005) as identified by Rex et al. [2004, 2006] and Manney et al. [2011] were not
379 associated with elevated North Pacific SSTs. Similarly, in the GEOS V2 CCM simulations, not
380 all winters forced by high North Pacific SSTs lead to late winter stratospheric cooling, because
381 stochastic atmospheric variability also plays a role in modulating the Arctic winter climate.
382
383 **Acknowledgements**
384 The authors thank Stacey Frith for providing the updated TOMS/SBUV data and processing the
385 model output, Markus Rex and Peter von der Gathen for supplying V_{PSC} timeseries, Alexey
386 Karpechko for helpful comments, and NASA's ACMAP program for funding.
387

References

Bosilovich, M. (2008), NASA'S modern era retrospective–analysis for research and applications: integrating earth observations, Earthzine, 26 September 2008.

Bloom, S., et al. (2005), Documentation and validation of the Goddard Earth–Observing System (GEOS) Data Assimilation System Version 4, Tech. Rep. 104606, V26, NASA, Greenbelt, Maryland, USA.

Butler, A. H., and L. M. Polvani (2011), El Niño, La Niña, and stratospheric sudden warmings: A reevaluation in light of the observational record, Geophys. Res. Lett., 38, L13807, doi:10.1029/2011GL048084.

Charlton, A., and L. Polvani (2007), A new look at stratospheric sudden warmings. Part I: Climatology and modeling benchmarks, J. Clim., 20, 449–469, doi:10.1175/JCLI3996.1.

Cohen, J., and J. Jones (2012), Tropospheric Precursors and Stratospheric Warmings, J. Climate, 24, doi: 10.1175/2011JCLI4160.1.

Frankignoul, C., and N. Sennéchael (2007), Observed influence of North Pacific SST anomalies on the atmospheric circulation, J. Climate, 20, 592–606.

Garfinkel, C. I., and D. L. Hartmann (2008), Different ENSO Teleconnections and Their Effects on the Stratospheric Polar Vortex, J. Geophys. Res. Atmos, 113, D18114, doi:10.1029/2008JD009920.

Garfinkel, C. I., D. L. Hartmann, and F. Sassi (2010), Tropospheric precursors of anomalous northern hemisphere stratospheric polar vortices, J. Climate, 23.

Hurwitz, M. M., P. A. Newman, and C. I. Garfinkel (2011a), The Arctic Vortex in March 2011: A Dynamical Perspective, Atm. Chem. Phys., 11, 11447–11453, doi:10.5194/acp–11–11447–2011.

Hurwitz, M. M., I.–S. Song, L. D. Oman, P. A. Newman, A. M. Molod, S. M. Frith, and J. E. Nielsen (2011b), Response of the Antarctic Stratosphere to Warm Pool El Niño Events in the GEOS CCM, Atm. Chem. Phys., 11, 9659-9669, doi:10.5194/acp-11-9659-2011.

Jadin, E. A., R. Wei, Y. A. Zyalyaeva, W. Chen, and L. Wang (2010), Stratospheric wave activity and the Pacific Decadal Oscillation, J. Atm. Solar–Terrestrial Phys., 72, 1163–1170, doi:10.1016/j.jastp.2010.07.009.

Manney, G. L., et al. (2011), Unprecedented Arctic ozone loss in 2011, Nature, doi:10.1038/nature10556.

Nakamura, H., G. Lin, and T. Yamagata (1997), Decadal climate variability in the North Pacific during the recent decades, B. Am. Meteorol. Soc., 78, 2215–2225.

Newman, P. A., E. R. Nash, and J. E. Rosenfield (2001), What controls the temperature of the Arctic stratosphere during the spring?, J. Geophys. Res., 106, 19999–20010.

Nishii, K., H. Nakamura, and Y. J. Orsolini (2010), Cooling of the wintertime Arctic stratosphere induced by the western Pacific teleconnection pattern, Geophys. Res. Lett., 37, L13805, doi:10.1029/2010GL043551.

Orsolini, Y. J., A. Y. Karpechko, and G. Nikulin (2009), Variability of the Northern Hemisphere polar stratospheric cloud potential: the role of North Pacific disturbances, Q. J. R. Meteorol. Soc., 135, 1020-1029, doi:10.1002/qj.409.

Pawson, S., and B. Naujokat (1999), The cold winters of the middle 1990s in the northern lower stratosphere, J. Geophys. Res., 104, 14209–14222.

Rayner, N. A., Parker, D. E., Horton, E. B., Folland, C. K., Alexander, L. V., Rowell, D. P., and Kaplan, A. (2003), Global analyses of sea surface temperature, sea ice, and night marine air

449 temperature since the late nineteenth century, J. Geophys. Res., 108, 4407,
450 doi:10.1029/2002JD2670.
451
452 Rex, M., Salawitch, R. J., von der Gathen, P., Harris, N. R. P., Chipperfield, M. P., and
453 Naujokat, B. (2004), Arctic ozone loss and climate change, Geophys. Res. Lett., 31, L04116,
454 doi:10.1029/2003GL018844.
455
456 Rex, M., et al. (2006), Arctic winter 2005: implications for stratospheric ozone loss and climate
457 change, Geophys. Res. Lett., 33, L23808, doi:10.1029/2006GL026731.
458
459 Rienecker, M. M., et al. (2011), MERRA – NASA's Modern– Era Retrospective, Anal. Res.
460 Appl., J. Climate, 24, 3624–3648, doi:10.1175/JCLID-11-00015.1.
461
462 SPARC CCMVal (2010), SPARC Report on the Evaluation of Chemistry–Climate Models,
463 edited by: Eyring, V., Shepherd, T. G., and Waugh, D. W., SPARC Report No. 5, WCRP-132,
464 WMO/TDNo. 1526, available online at: http://www.atmosp.physics.utoronto.ca/SPARC.
465
466 Stolarski, R. S., and S. M. Frith (2006), Search for evidence of trend slow–down in the long-term
467 TOMS/SBUV total ozone data record: the importance of instrument drift uncertainty, Atmos.
468 Chem. Phys., 6, 4057–4065, doi:10.5194/acp–6–4057–2006.
469
470 World Meteorological Organization (WMO) (2011), Scientific assessment of ozone depletion:
471 2010, Global Ozone Research and Monitoring Project, Rep. No. 52, 516 pp., Geneva,
472 Switzerland.
473
474 Woollings, T., Charlton–Perez, A., Ineson, S., Marshall, A. G., and Masato, G. (2010),
475 Associations between stratospheric variability and tropospheric blocking, J. Geophys. Res., 115,
476 D06108, doi:10.1029/2009JD012742.
477

Table and Figure Captions

Table 1: Number of events and days when eddy heat flux at 40–80°N, 100hPa $\geq$ 25 K m s^{-1}, for the High and Low ensembles.

Table 2: Simulated number and frequency of winters with at least one SSW (2^{nd} and 3^{rd} columns), and number and of winters with two SSWs (4^{th} and 5^{th} columns). 40 winters for each of the High, Low and ENSO neutral simulations are considered. The 6^{th} column shows the frequency of active winters during the 1979–2011 period, based on a list of historical SSWs [Butler and Polvani, 2011]. For the historical SSWs, the four years with the highest (lowest) January/February North Pacific SSTs represent the High (Low) case.

Table 3: Ensemble and monthly mean area where 50–hPa polar temperature is less than 195 K [10^6 m^2]. Differences between the High and Low areas are significantly significant at the 90% level, in a two–tailed t–test, in January, February and March.

Figure 1: (a) Timeseries of the January/February mean North Pacific SST index. Blue (cyan) stars denote winters used to construct the High (Low) SST and sea ice boundary conditions. The red star denotes the North Pacific SST index in 2011. (b) Timeseries of North Pacific SST anomalies through the extended winter season, for High – Low (black line) and 2010–2011 anomalies (red line). (c) January/February mean SSTs used as boundary conditions in the High ensemble. (d) January/February mean differences between the High and Low SST fields. Gray contours indicate zero difference. Black boxes in (c) and (d) indicate the North Pacific region.

Figure 2: High – Low geopotential height differences [m] at Northern Hemisphere mid– and high latitudes at 850 hPa (left column), 300 hPa (center column) and 50 hPa (right column), in (a–c) December and (d–f) March. Note the different color scale for each pressure level. White contours indicate zero difference. Gray dashed contours show geopotential heights in the ENSO neutral simulation. Black wedges indicate the North Pacific region. All of the major features are statistically significant at the 95% level, in a two–tailed t–test.

Figure 3: Upper panel: Eddy heat flux [K m s^{-1}] at 40–80°N, 100 hPa in the preceding 45 days. Solid blue and cyan lines indicate the High and Low ensemble mean values. Dashed blue and cyan lines indicate the 3rd–highest and lowest values of each ensemble. Days when the High – Low eddy heat flux difference is significant at the 95% (80%) level are indicated by the black (gray) Xs below the plot. Days when the difference in variability between the High and Low ensembles is significant at the 95% (80%) level are indicated by the black (gray) Xs above the plot. Center panel: Like the upper panel, but for polar cap temperature [K] at 50 hPa. Lower plot: High – Low ensemble mean differences in eddy heat flux (dotted black line) and temperature (solid black line).

Figure 4: Histograms of the January–February–March (JFM) seasonal mean polar cap temperature [K] at 50 hPa: (a) High and Low ensembles, and (b) QBO–easterly years and QBO–westerly years. The black–tipped bars indicate the location of the ensemble mean values; the High and Low ensemble mean difference is significant at the 95% level, in a two–tailed t–test.

Figure 5: High – Low temperature differences [K] at 80°N, as a function of date and altitude. White contours indicate zero difference. Black Xs indicate differences significant at the 95% confidence level, in a two–tailed t–test.

Figure 6: January/February North Pacific SST anomaly [K] as a function of February/March V_{PSC} in the 380–550 K layer [10^6 km^3], for the 1980–2011 period. SST anomaly and V_{PSC} values are denoted by year number (e.g., '11' denotes 2011).

Figure 7: Zonally asymmetric component of the 300–hPa geopotential height anomalies in the 5–20 days preceding SSWs in the High and Low ensembles. White contours indicate zero difference.

Figure 8: High – Low ozone differences [ppmv] at 80°N, as a function of date and altitude. White contours indicate zero difference. Black (gray) Xs indicate differences significant at the 95% (80%) confidence level, in a two–tailed t–test.

538 **Figure 9**: Timeseries of zonal mean temperature at 80°N, 50 hPa during the 2010–2011 winter
539 (black), as compared with the High (blue) and Low (cyan) ensemble means. 195 K is denoted by
540 the dotted black line.
541
542 **Figure 10**: April total ozone differences [DU] (a) for the High – Low ensemble means and (b)
543 2011 – climatology from the TOMS/SBUV dataset. In (a), black Xs indicate differences
544 significant at the 95% level in a two–tailed t–test. White letters denote the approximate location
545 of the four cities: London, Moscow, Calgary and Washington.
546
547 **Figure 11**: April UV index in four cities: Washington (approximately 283°E, 38°N), Calgary
548 (246°E, 51°N), Moscow (37°E, 55°N) and London (0°E, 51°N). For each city, the first five
549 vertical bars represent the UV index calculated based on April total ozone from the
550 TOMS/SBUV dataset, for 1987 (unusually low North Pacific SSTs), 1988 (low), 1991 (high),
551 1997 (high) and 2011 (high). The last two vertical bars represent the mean UV index calculated
552 based on April total ozone for the High and Low simulations. Differences in the April UV index
553 between the High and Low ensembles are significant at the 95% confidence level in Washington
554 and at the 90% confidence level in London, in two–tailed t–tests.
555

555 **Tables**

556

	# of Events	# of Days				
	Total	Total	Dec	Jan	Feb	Mar
High	143	414	89	82	48	84
Low	153	497	138	91	103	51

557

558 **Table 1**: Number of events and days when eddy heat flux at 40–80°N, 100hPa $\geq$ 25 K m s^{-1},
559 between December and March, for the High and Low ensembles. Totals represent the
560 November–March extended winter season.

561

	GEOS V2 CCM Simulations				1979–2011
	# of Active Winters	Frequency of Active Winters	# of Winters with Two SSWs	Frequency of Two–SSW Winters	Frequency of Active Winters
High	7	0.18	2	0.05	0
Low	20	0.50	2	0.05	1
ENSO Neutral	10	0.25	0	0	0.42

562

563 **Table 2**: Simulated number and frequency of winters with at least one SSW (2^{nd} and 3^{rd}
564 columns), and number and of winters with two SSWs (4^{th} and 5^{th} columns). 40 winters for each
565 of the High, Low and ENSO neutral simulations are considered. The 6^{th} column shows the
566 frequency of active winters during the 1979–2011 period, based on a list of historical SSWs
567 [Butler and Polvani, 2011]. For the historical SSWs, the four years with the highest (lowest)
568 January/February North Pacific SSTs represent the High (Low) case.

569

569

	Dec	Jan	Feb	Mar
High	2.6 ± 1.2	19.2 ± 2.6	27.3 ± 2.5	12.1 ± 2.2
Low	3.7 ± 1.2	11.4 ± 2.5	16.4 ± 2.8	6.9 ± 1.7

570

571 **Table 3**: Ensemble and monthly mean area where 50–hPa polar temperature is less than 195 K
572 [10^6 m^2]. Differences between the High and Low areas are significantly significant at the 90%
573 level, in a two–tailed t–test, in January, February and March.

574

574 **Figures**

575

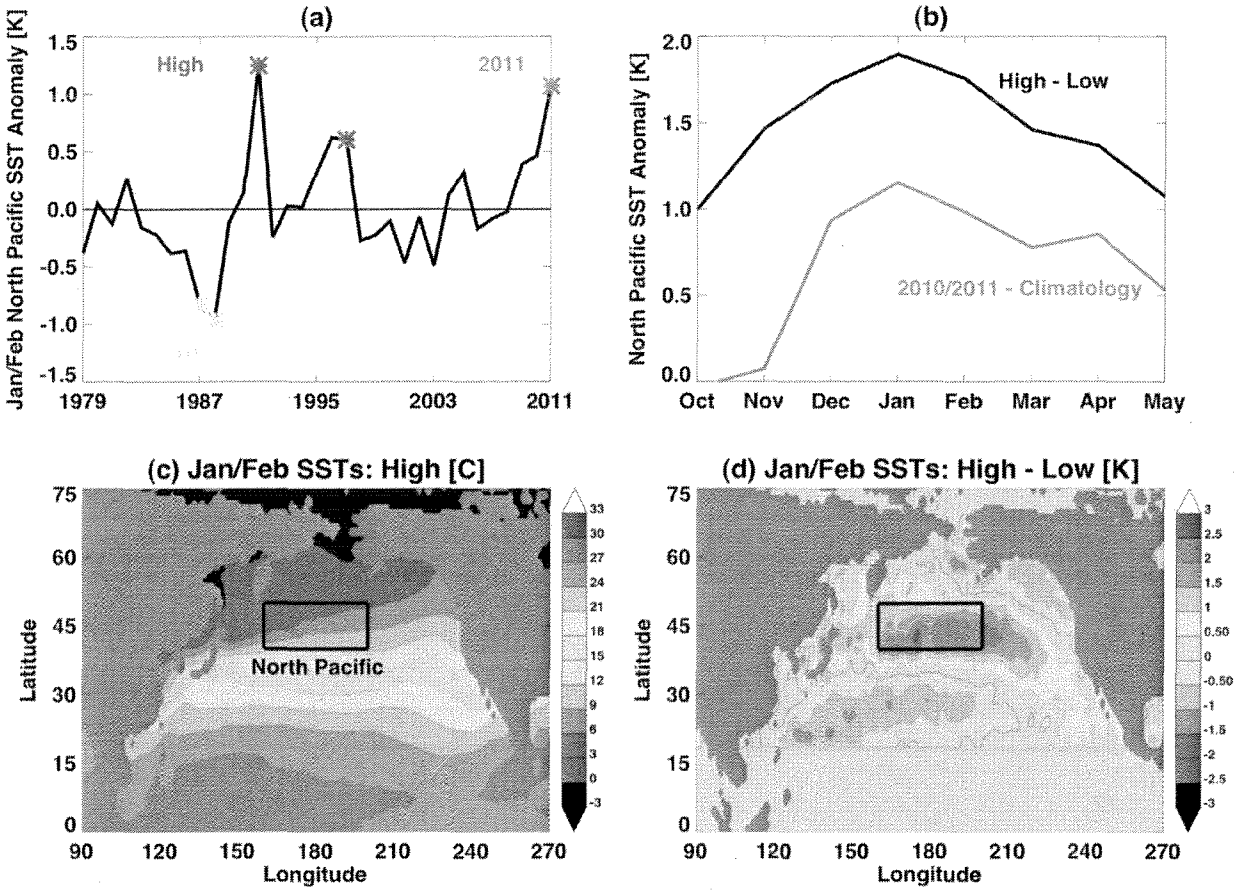

576

577 **Figure 1**: (a) Timeseries of the January/February mean North Pacific SST index. Blue (cyan)
578 stars denote winters used to construct the High (Low) SST and sea ice boundary conditions. The
579 red star denotes the North Pacific SST index in 2011. (b) Timeseries of North Pacific SST
580 anomalies through the extended winter season, for High – Low (black line) and 2010–2011
581 anomalies (red line). (c) January/February mean SSTs used as boundary conditions in the High
582 ensemble. (d) January/February mean differences between the High and Low SST fields. Gray
583 contours indicate zero difference. Black boxes in (c) and (d) indicate the North Pacific region.

584

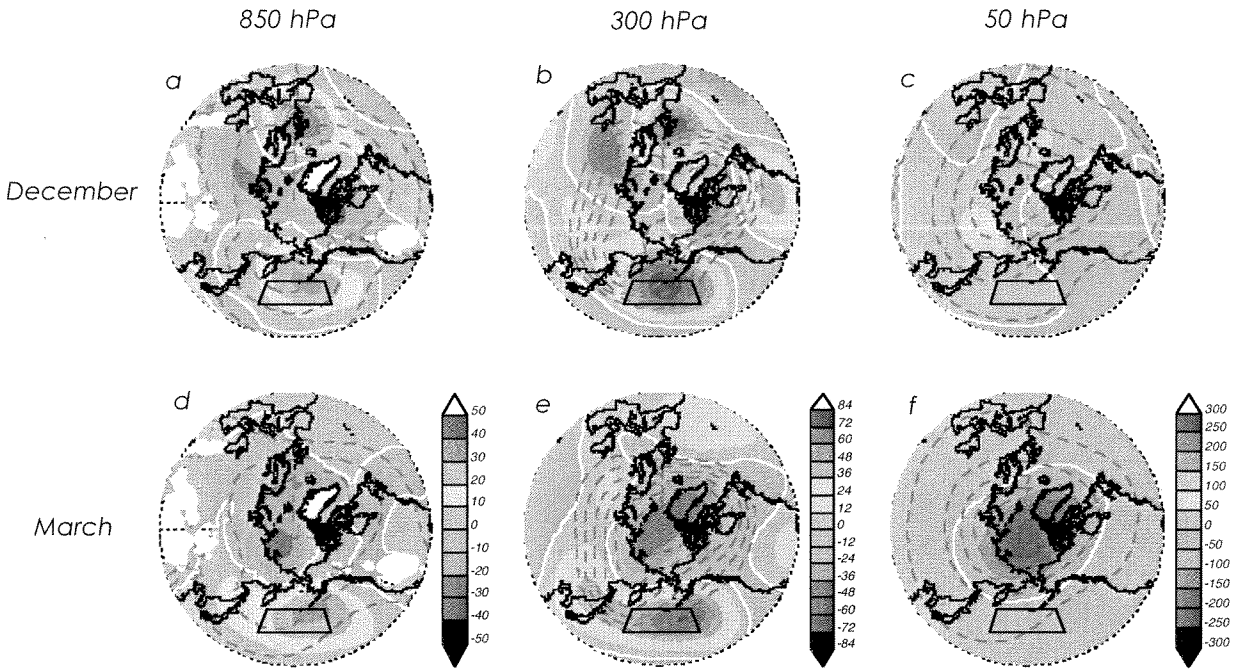

584

585 **Figure 2**: High – Low geopotential height differences [m] at Northern Hemisphere mid– and
586 high latitudes at 850 hPa (left column), 300 hPa (center column) and 50 hPa (right column), in
587 (a–c) December and (d–f) March. Note the different color scale for each pressure level. White
588 contours indicate zero difference. Gray dashed contours show geopotential heights in the ENSO
589 neutral simulation. Black wedges indicate the North Pacific region. All of the major features are
590 statistically significant at the 95% level, in a two–tailed t–test.

591

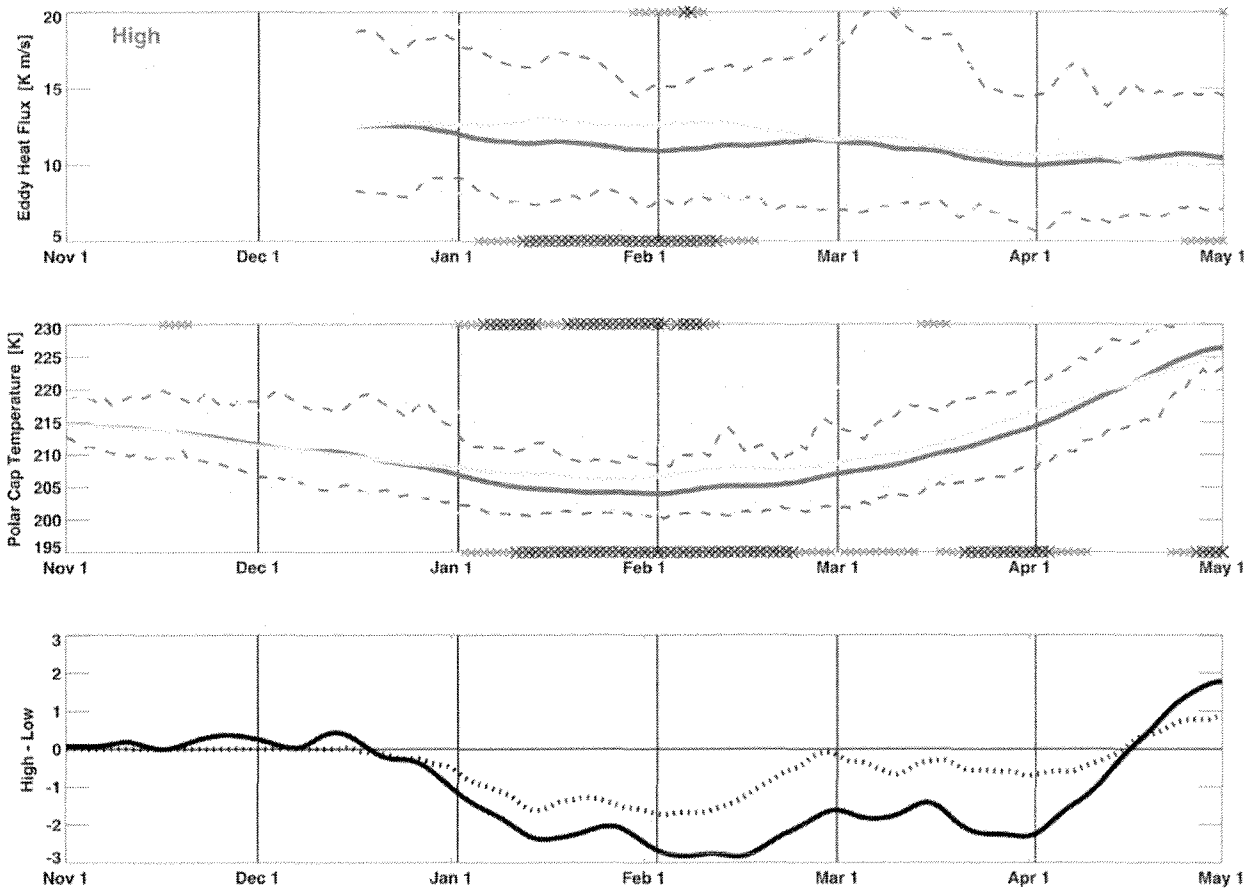

591

592 **Figure 3**: Upper panel: Eddy heat flux [K m s^{-1}] at 40–80°N, 100 hPa in the preceding 45 days.
593 Solid blue and cyan lines indicate the High and Low ensemble mean values. Dashed blue and
594 cyan lines indicate the 10^{th}– and 90^{th}–percentile values for each ensemble. Black (gray) Xs
595 below the plot indicate days when the High – Low eddy heat flux difference is significant at the
596 95% (80%) level, in a two–tailed t–test. Black (gray) Xs above the plot indicate days when the
597 difference in variability between the High and Low ensembles is significant at the 95% (80%)
598 level, in an F–test. Center panel: Like the upper panel, but for polar cap temperature [K] at 50
599 hPa. Lower plot: High – Low ensemble mean differences in eddy heat flux (dotted black line)
600 and temperature (solid black line).

601

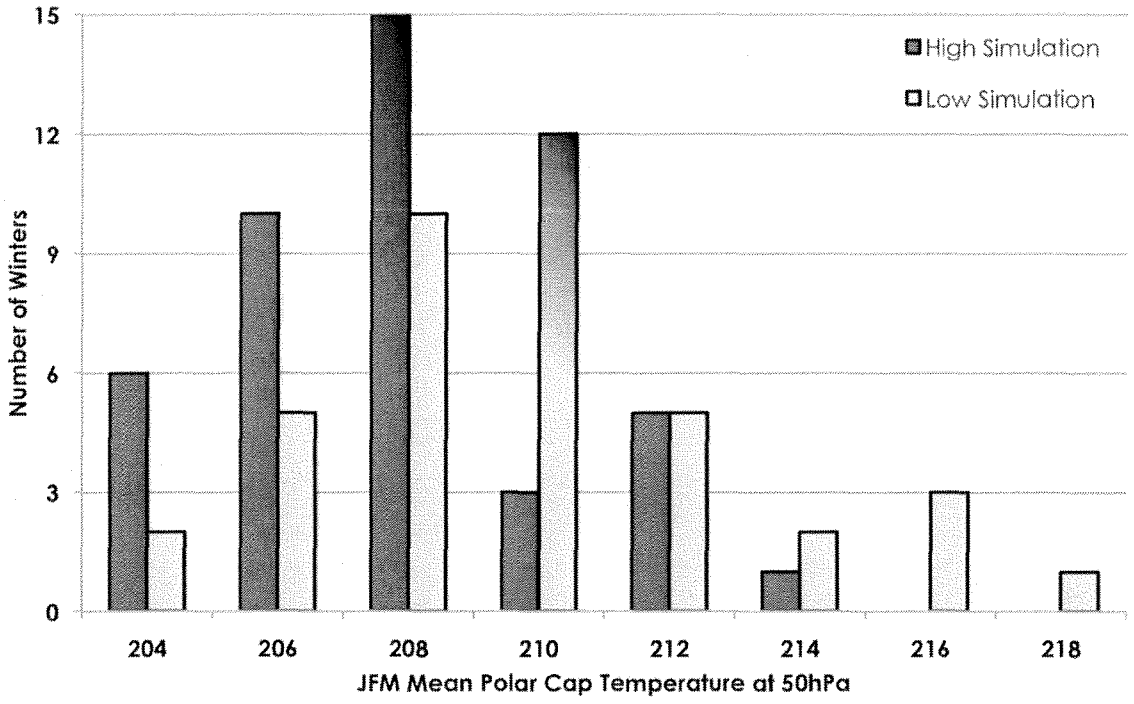

(a)

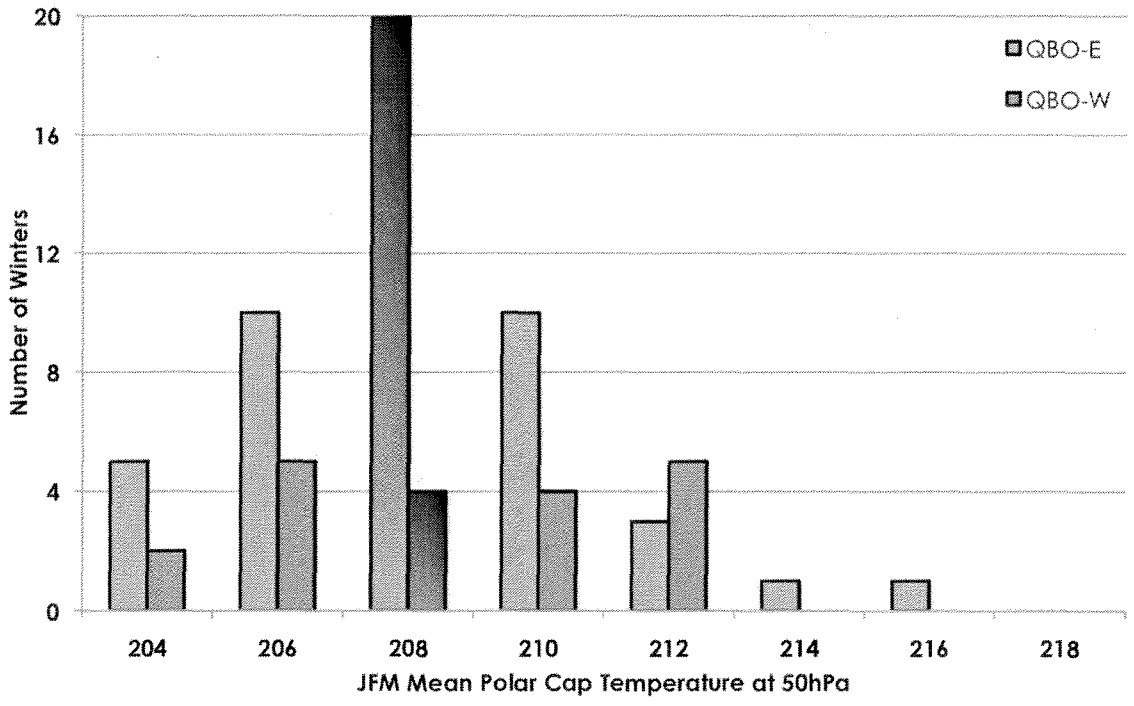

(b)

Figure 4: Histograms of the January–February–March (JFM) seasonal mean polar cap temperature [K] at 50 hPa: (a) High and Low ensembles, and (b) QBO–easterly years and QBO–westerly years. The black–tipped bars indicate the location of the ensemble mean values; the High and Low ensemble mean difference is significant at the 95% level, in a two–tailed t–test.

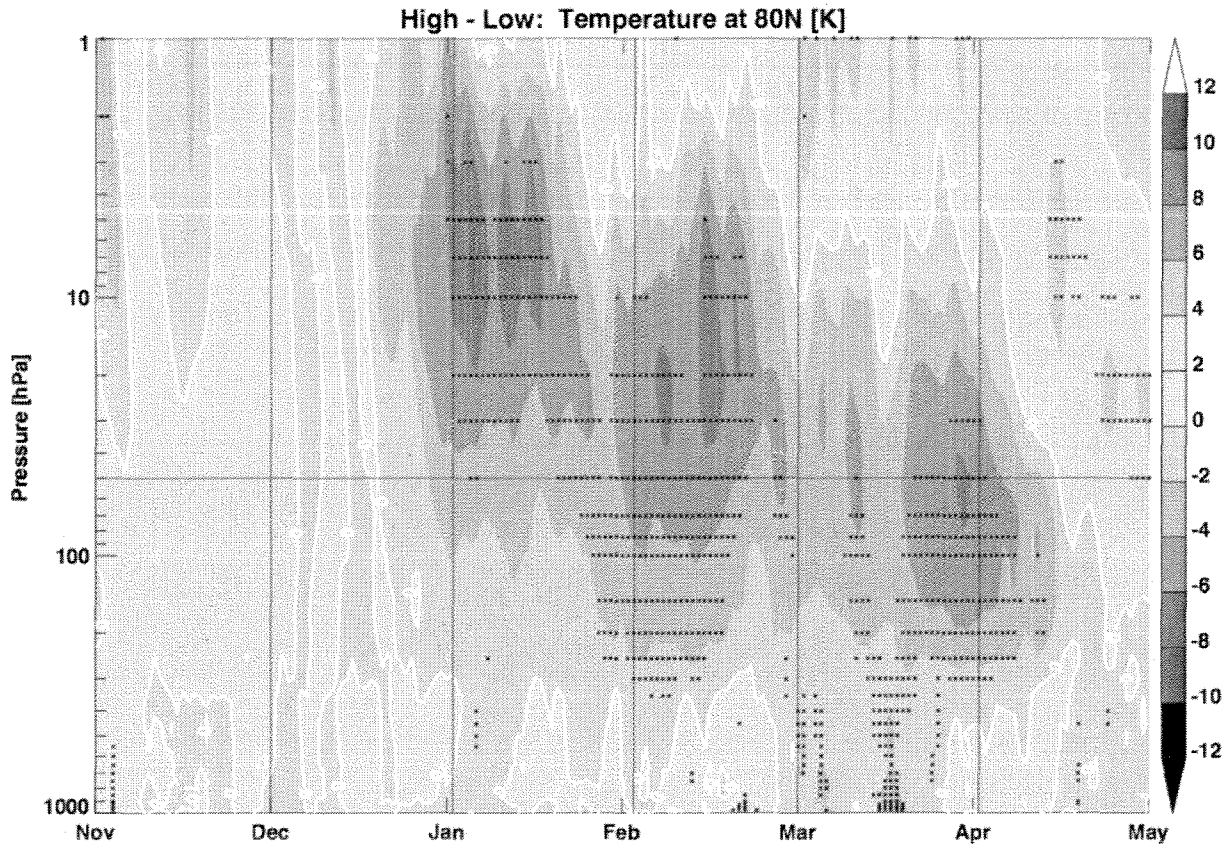

607

608 **Figure 5**: High – Low temperature differences [K] at 80°N, as a function of date and altitude.
609 White contours indicate zero difference. Black Xs indicate differences significant at the 95%
610 confidence level, in a two–tailed t–test.

611

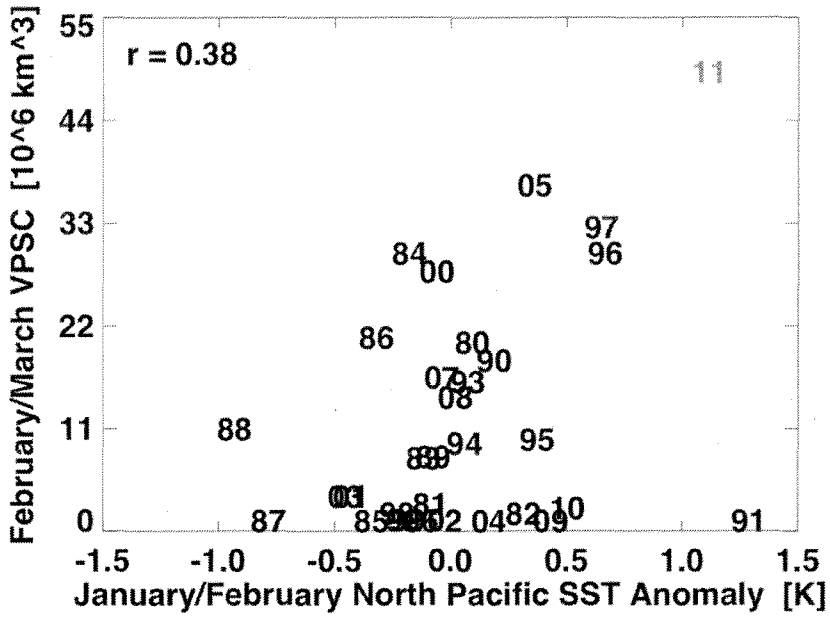

611

612 **Figure 6**: January/February North Pacific SST anomaly [K] as a function of February/March
613 V_{PSC} in the 380–550 K layer [10^6 km^3], for the 1980–2011 period. SST anomaly and V_{PSC}
614 values are denoted by year number (e.g., '11' denotes 2011).

615

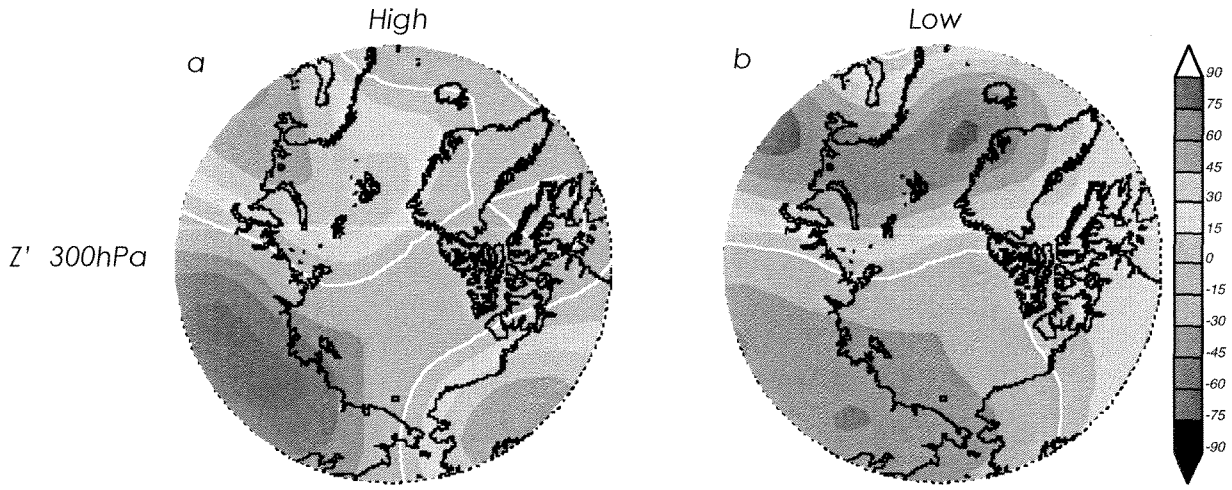

615

616 **Figure 7**: Zonally asymmetric component of the 300–hPa geopotential height anomalies in the
617 5–20 days preceding SSWs in the High and Low ensembles. White contours indicate zero
618 difference.

619

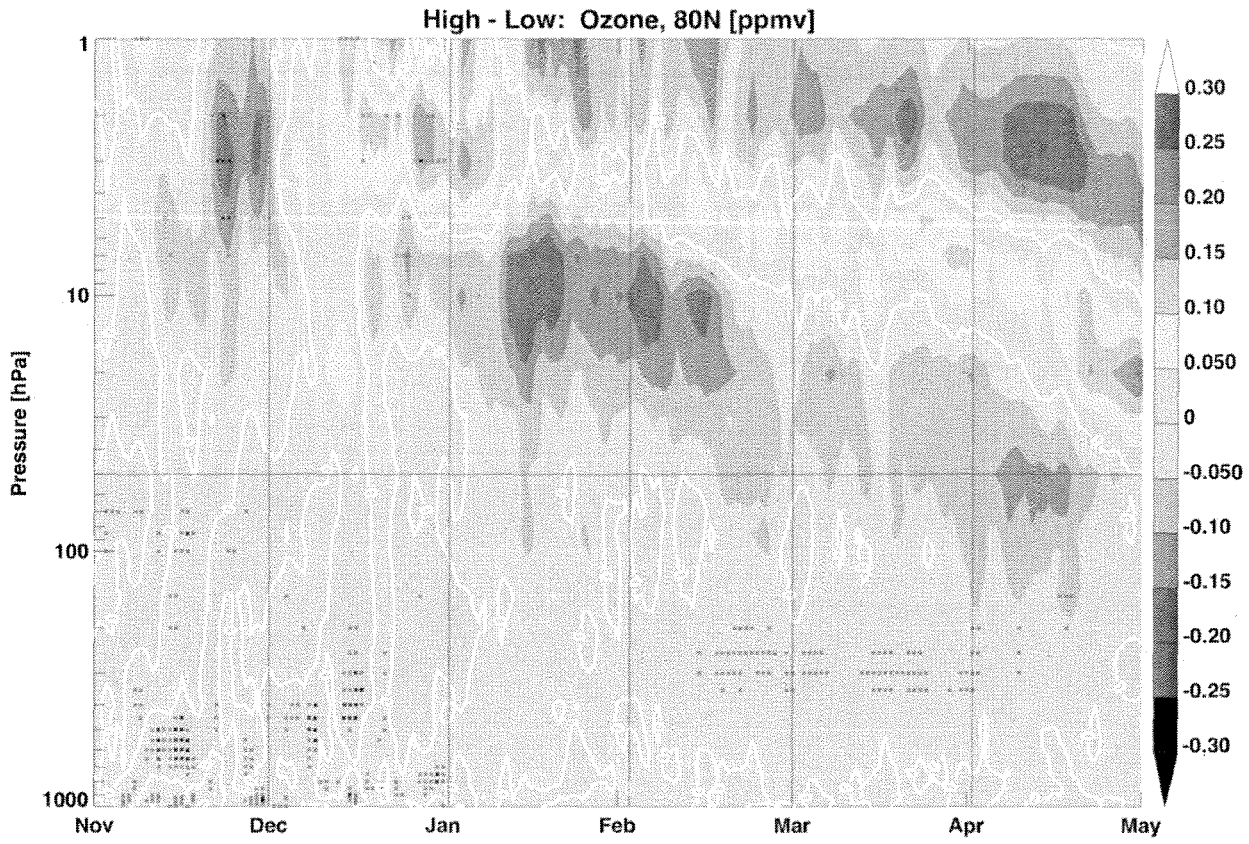

Figure 8: High – Low ozone differences [ppmv] at 80°N, as a function of date and altitude. White contours indicate zero difference. Black (gray) Xs indicate differences significant at the 95% (80%) confidence level, in a two–tailed t–test.

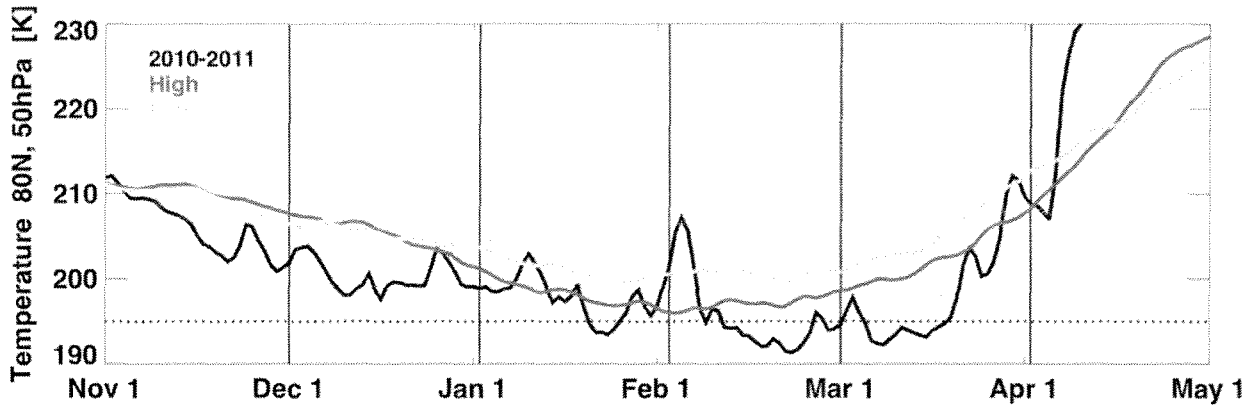

Figure 9: Timeseries of zonal mean temperature at 80°N, 50 hPa during the 2010–2011 winter (black), as compared with the High (blue) and Low (cyan) ensemble means. 195 K is denoted by the dotted black line.

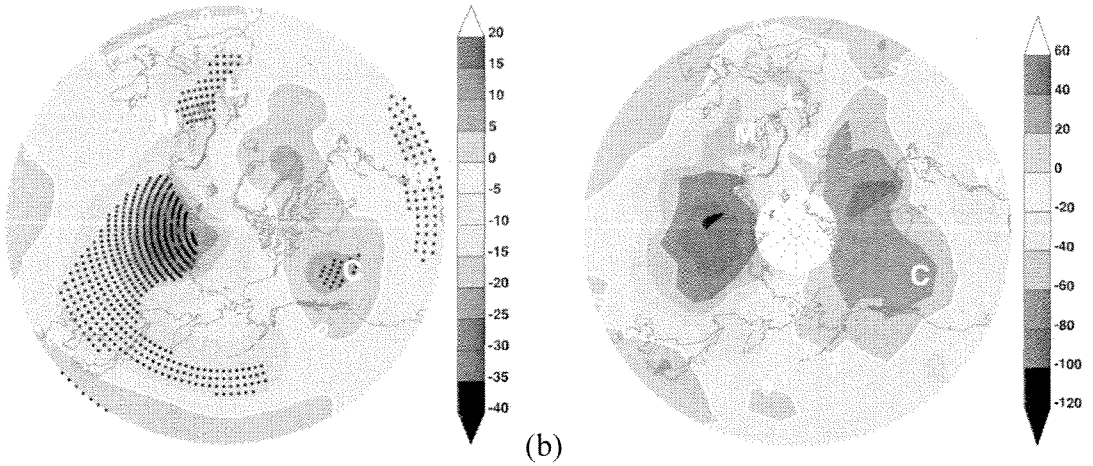

(a) (b)

Figure 10: April total ozone differences [DU] (a) for the High – Low ensemble means and (b) 2011 – climatology from the TOMS/SBUV dataset. In (a), black Xs indicate differences significant at the 95% level in a two–tailed t–test. White letters denote the approximate location of the four cities: London, Moscow, Calgary and Washington.

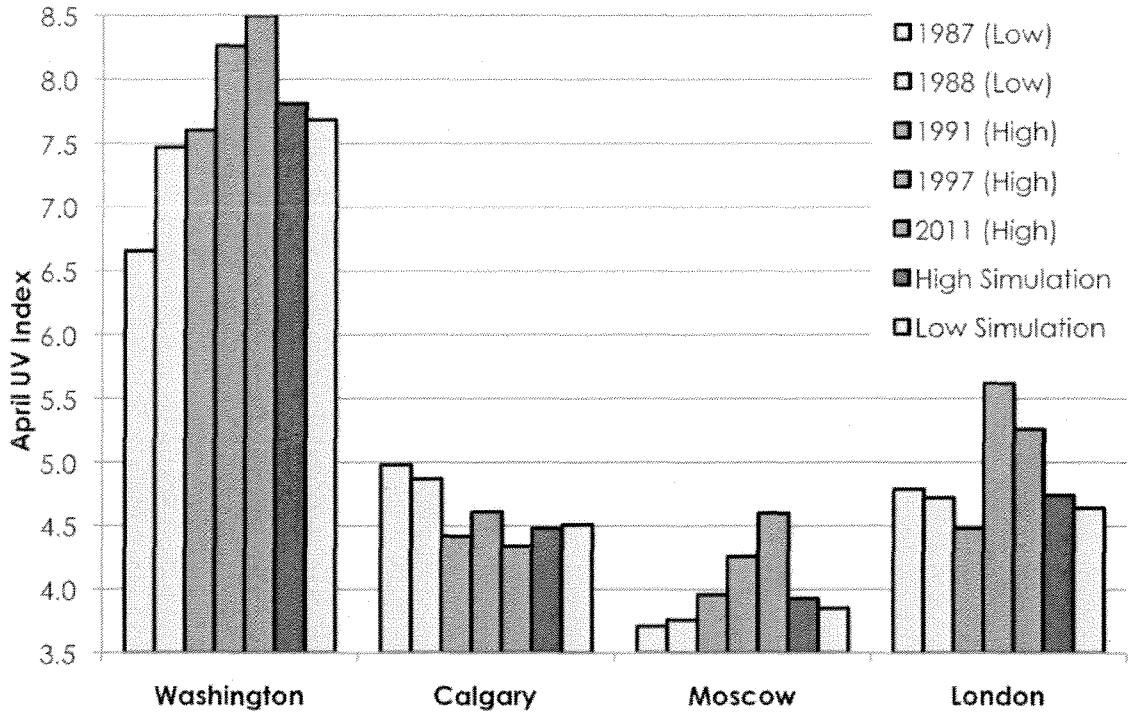

632

633 **Figure 11**: April UV index in four cities: Washington (approximately 283°E, 38°N), Calgary
634 (246°E, 51°N), Moscow (37°E, 55°N) and London (0°E, 51°N). For each city, the first five
635 vertical bars represent the UV index calculated based on April total ozone from the
636 TOMS/SBUV dataset, for 1987 (unusually low North Pacific SSTs), 1988 (low), 1991 (high),
637 1997 (high) and 2011 (high). The last two vertical bars represent the mean UV index calculated
638 based on April total ozone for the High and Low simulations. Differences in the April UV index
639 between the High and Low ensembles are significant at the 95% confidence level in Washington
640 and at the 90% confidence level in London, in two–tailed t–tests.